Hydrogen bond network modes in liquid water

David P. Shelton *

Department of Physics and Astronomy, University of Nevada, Las Vegas, Nevada 89154-4002, USA

(Received 30 December 2022; revised 11 June 2023; accepted 2 November 2023; published 21 November 2023)

Collective modes and dynamics of dense disordered materials such as water are not well understood, but nonlinear optics provides a sensitive probe to study polar modes in these materials. Here we report the hyper-Raman (HRS) light scattering spectrum measured for liquid D_2O decomposed into contributions from transverse and longitudinal dipolar modes and octupolar modes, using the polarization dependence of HRS. Transverse HRS is observed for orientation and stretching modes, while longitudinal HRS is observed for translation, libration, and bending modes. The HRS observations indicate molecular correlation at distances >200 nm for all modes of orientation, libration, and vibration. The rocking/wagging, twisting, and translation modes for D_2O molecules in the hydrogen bonded network are distinguished. The LO-TO splitting is 28 cm^{-1} for the libration mode and 16 cm^{-1} for the translation mode, and the relaxation time for libration modes is about 80 fs. The long-range correlation of the orientation and stretching modes is explained as the result of the dipole-dipole orientation correlation in a dipolar fluid. The long-range correlation of the longitudinal polarized libration and bending modes needs further study.

DOI: 10.1103/PhysRevB.108.174203

I. INTRODUCTION

The many anomalous properties of liquid water are the result of a disordered network of strong directional hydrogen bonds between the molecules, and the structure and dynamics of liquid water remains a subject of research [1]. Among the many experimental techniques applied to study water, structure has been determined by x-ray and neutron diffraction [2], and dynamics has been probed by dielectric, infrared, and Raman spectroscopy [3–7]. Theoretical approaches include classical molecular dynamics simulation [8–11] and more recently *ab initio* molecular dynamics simulation [12–17], but the combination of nuclear quantum effects and cooperative hydrogen bond interactions make water a difficult problem.

The stretching and bending vibrations of water molecules in the liquid are strongly perturbed versions of the single-molecule vibrations in the gas phase, but the free translation and rotation of molecules in the gas phase are replaced by hindered translation and libration modes of collective vibration of the hydrogen-bonded molecules and slow diffusion of molecular orientation which have no counterpart in the single-molecule spectrum. These vibrations in liquid water may be similar to the lattice modes of ordinary ice Ih [18–20]. The proton disorder in ice Ih complicates a normal mode analysis, but measurements and mode calculations for proton-ordered ice XI indicate that the libration modes are delocalized and propagating [21,22]. Recent molecular dynamics simulations for liquid water also found dispersive optical phonon-like modes in the libration and OH-stretching bands, indicating similarity of the dynamics in ice and water [9]. However, existing experimental methods do not unequivocally determine the nature of the modes in liquid water.

Hyper-Raman scattering (HRS) is the process where a Raman-shifted photon is emitted following excitation of the system by a pair of photons. The dependence of HRS on the polarization of the incident and scattered light can be used to separate the contributions of TO (transverse optical) and LO (longitudinal optical) phonon modes for dipolar vibrations, and HRS has been used to investigate vibrational excitations in crystals, glasses, and liquids [23]. Recently the HRS spectra for H_2O and D_2O water and ice without polarization selection [24], and H_2O with polarization selection [25], were measured to study the intermolecular vibrations. Other recent HRS measurements for several glasses and molecular liquids with polarization selection have found transverse and longitudinal nonlocal vibration modes with correlation over distances comparable to the wavelength of the scattering wave vector [23,26–29].

The present work applies polarized HRS spectral measurement techniques and analysis, developed in previous studies of long-range correlation in liquids, to the study of water. HRS is used to separate TO and LO contributions to the libration band which are unresolved or unobserved by other spectroscopic techniques, and to assess the extent of nonlocal spatial correlation for the modes.

II. EXPERIMENT

The experiment measures scattered light that is Raman-shifted from the laser second harmonic frequency. Linearly polarized pulses from an injection-seeded, cavity-dumped, single longitudinal mode Nd:YAG (yttrium aluminium garnet) laser (operating at $\lambda = 1064$ nm, 10 kHz repetition rate, 6 ns pulse duration, 100 MHz = 0.003 cm^{-1} linewidth) are

*shelton@physics.unlv.edu

focused to an 8 μm diameter beam waist in the liquid sample in a standard square 10 mm fluorimeter cuvette. Scattered light at $\theta = 90^\circ$ was collected and collimated by an aspheric lens ($f = 4$ mm), analyzed by a linear polarizer, focused into an optical fiber, and fiber-coupled to the scanning grating spectrometer and photon-counting detector. The background count rate of the gated photomultiplier was $0.0010\,s^{-1}$. The sample cell temperature was 25 °C for all measurements, and the average laser beam power in the sample was 2 W. D_2O was chosen to reduce laser beam absorption and thermal lensing effects, but the sample temperature at the focus is increased to 29 °C (see Supplemental Material [30] and Refs. [31–33] therein). The D_2O sample (25 MΩ cm) flows in a loop containing the sample cell, conductivity cell, ion exchange resin column, and 0.2 μm dust filter. The 2 M KCl solution sample was filtered into a sealed cuvette.

Spectra for polarization analysis were acquired from sequential scans with VV, HH, VH, and HV polarization, repeated up to 600 times, and summed for each polarization configuration. Scattering configurations with incident and scattered light polarized either perpendicular or parallel to the horizontal scattering plane are denoted VV, HV, VH, and HH, where V denotes vertical linear polarization, H denotes horizontal linear polarization, and the first and second letters refer to the incident and scattered light, respectively. Spectra were acquired with numerical aperture NA = 0.375 and corrected for the effects of detector dead time and the finite collection aperture (see Supplemental Material [30] and Refs. [34–36] therein). The spectrometer response has strong polarization dependence, so an effective depolarizer is required between the analyzing polarizer and the spectrometer. The combination of a long multimode fiber (40 m) followed by a liquid crystal polymer microarray depolarizer was used. The polarization and spectral response of the system was calibrated using a thermal light source and integrating sphere placed at the sample position. The spectrometer spectral slit width (SSW) was $20\,cm^{-1}$ for most measurements. Further experimental details are provided in the Supplemental Material [30].

III. HYPER-RAMAN SCATTERING

HRS is produced by the oscillating molecular dipoles $\mu = \beta E_\omega^2$ induced by the applied laser field E_ω, where the material response tensor β must have odd parity and vanishes for centrosymmetric molecules. Vibrational modulation of β results in a dipole oscillation frequency shifted from the laser second harmonic frequency. HRS from a liquid of uncorrelated randomly oriented molecules is the incoherent sum of the individual molecule HRS intensities, but HRS is very sensitive to local and nonlocal molecular orientation correlations.

The third rank molecular first hyperpolarizability tensor β which mediates HRS can be expressed in Cartesian tensor form or as the sum of irreducible spherical tensors [37]. The first rank irreducible spherical tensor contribution to β transforms as a vector and produces pure dipolar HRS for which $I_{VV}/I_{HV} = 9$, and the third rank irreducible spherical tensor contribution produces pure octupolar HRS for which $I_{VV}/I_{HV} = 3/2$. HRS due to the first rank irreducible spherical tensor contribution to β is sensitive to polar modes and correlations.

The vector β contributions for the molecules in a liquid form a homogeneous, isotropic, random vector field. The most general correlation tensor for such a field, in diagonal form, has transverse and longitudinal correlation functions as the diagonal components, and produces HRS scattering with components polarized longitudinal and transverse to the scattering wave vector [38]. Vector field correlations do not affect the octupolar β HRS contribution. The HRS intensities for 90° scattering, including the vector and octupolar contributions, are given by [38]

$$I_{VV} = (3/2)A_O + 9A_T, \tag{1}$$

$$I_{HV} = A_O + A_T, \tag{2}$$

$$I_{HH} = I_{VH} = A_O + (1/2)(A_T + A_L), \tag{3}$$

where A_O is the octupolar contribution, A_T is the transverse dipolar contribution, and A_L is the longitudinal dipolar contribution. The polarized HRS data at each frequency are combined to determine A_O, A_T, and A_L at that frequency using the following relations:

$$A_O = (6/5)I_{HV} - (2/15)I_{VV}, \tag{4}$$

$$A_T = (2/15)I_{VV} - (1/5)I_{HV}, \tag{5}$$

$$A_L = (2/15)I_{VV} - (11/5)I_{HV} + I_{VH} + I_{HH}. \tag{6}$$

The noise in the spectral data is increased using Eqs. (4)–(6), with the largest increase for A_L.

The HRS intensities A_T and A_L are determined by the spatial Fourier transform of the correlation tensor for vector β, Eqs. (11) and (12) of Ref. [38]. In the case where intermolecular correlations are short range or absent, $A_T = A_L$. Unequal intensities for A_T and A_L requires correlation at distances comparable to or larger than the wavelength of the scattering wavevector. An explicit example is shown in Fig. 4 of Ref. [39] for the correlation function of a solenoidal vector field with r^{-3} asymptotic dependence, for which $A_L = 0$. HRS intensity ratio $I_{HV}/I_{VH} \neq 1$ is an indicator for a dipolar mode with long-range correlation, ranging from 2 for a pure transverse dipole mode to 0 for a pure longitudinal dipole mode.

The A_O, A_T, and A_L spectra are fitted with the sum of Lorentzian functions

$$I_j(\Delta\nu) = A_j/[1 + (\Delta\nu/\Delta\nu_j)^2], \tag{7}$$

except for the stretching mode which was fitted with the sum of Gaussian functions

$$I_j(\Delta\nu) = A_j \exp[-(\Delta\nu/\Delta\nu_j)^2], \tag{8}$$

where $\Delta\nu = (\nu - \bar{\nu}_j)$ is the detuning from resonance at Stokes frequency shift ν for mode ν_j with frequency $\bar{\nu}_j$ and width $\Delta\nu_j$. The spectral profiles for the hydrogen bond network modes are considered to be the result of inhomogeneous broadening by variations of the local environment, convolved with homogeneous broadening by fast vibration relaxation. The excitations are delocalized and inhomogeneous, percolating through the network and dissipating by coupling to many similar modes at nearby frequency. The convolution is approximated by a sum of Lorentzian functions with life-

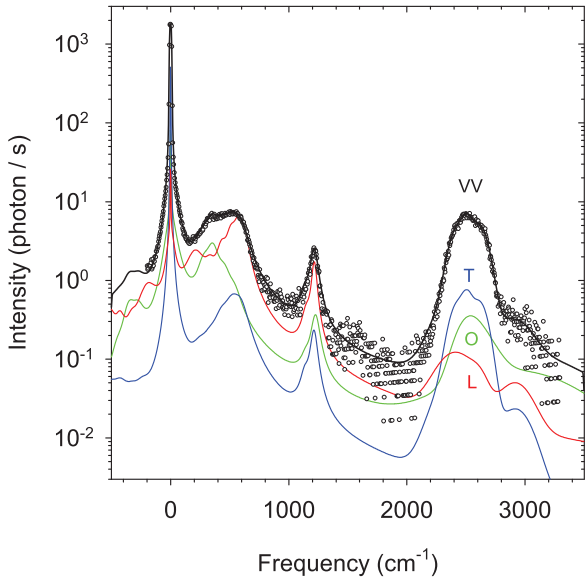

FIG. 1. The VV HRS spectrum of D_2O scanned with 20 cm^{-1} spectral resolution is shown by the data points (circles). T, O, and L spectra (blue, green, and red curves, respectively) are combined to form the VV spectrum (black curve) fitted to the data. Frequency ν is the Stokes Raman shift.

time broadened width $\Delta\nu_j(\mathrm{cm}^{-1}) = (2\pi c\tau)^{-1}$, where τ is the relaxation time.

The spectrum was multiplied by the factor

$$[1 + \exp(-hc\nu/kT)]^{-1} \tag{9}$$

to account for the Stokes/anti-Stokes asymmetry ($kT/hc = 207\,\mathrm{cm}^{-1}$ at 25 °C) and convolved with the spectrometer spectral slit function for the least-squares fit to the experimental data.

IV. EXPERIMENTAL RESULTS

The VV HRS spectrum for D_2O is shown in Fig. 1. The main spectral features are the orientation diffusion mode at 0 cm^{-1}, the hindered translation and libration modes below 800 cm^{-1}, the bending mode at 1215 cm^{-1}, and the symmetric and asymmetric stretching modes at about 2500 cm^{-1}. Shorter scans over each region with VV, HH, VH, and HV polarization were used to obtain the transverse (T) and longitudinal (L) dipolar and the octupolar (O) contributions to the HRS spectrum. Figure 2 shows the T, L, and O contributions obtained from the HRS polarization data (Fig. S4 of the Supplemental Material [30]) in the spectral band for the orientation, translation, and libration modes. The solid curves marked T, L, and O in Fig. 1 are obtained by combining the results in Fig. 2 and similar results obtained for the bending and stretching bands. Additional graphs of the data and details of the fit functions are in the Supplemental Material [30].

Results for A_O/A_T and A_L/A_T are given in Table I at frequencies for orientation (0 cm^{-1}), libration (590 cm^{-1}), bending (1215 cm^{-1}), and stretching (2500 cm^{-1}). Long-range correlation for a mode is indicated by deviation from $A_L/A_T = 1$ for that mode, and all the modes in Table I show significant long-range correlation.

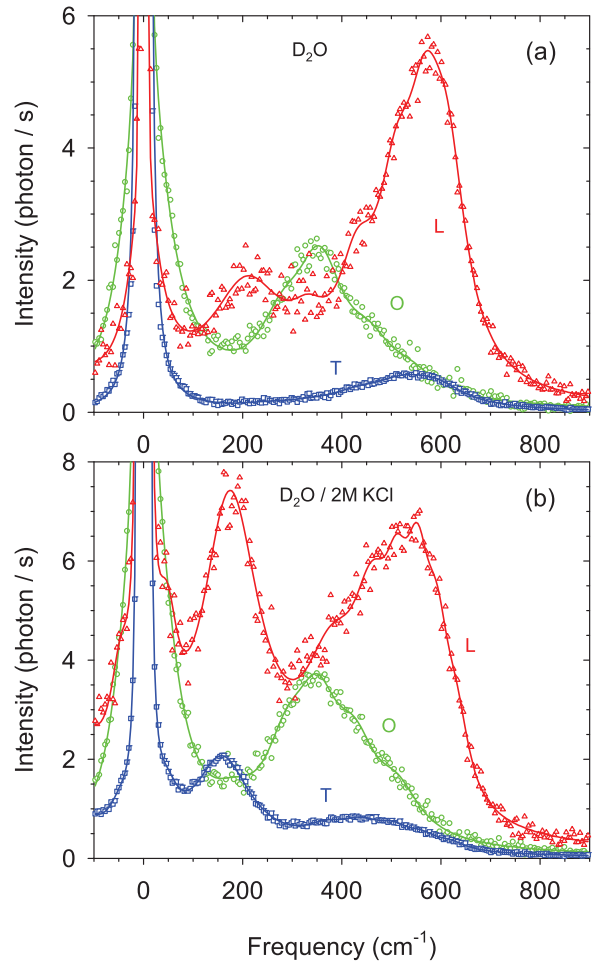

FIG. 2. A_0, A_T, and A_L (O, T, and L) spectra for (a) D_2O and (b) D_2O solution with 2 M KCl. The solid curves are fitted to the data points for the T (blue squares), O (green circles), and L (red triangles) spectra. The data points were obtained by combining intensities measured with four linear polarization configurations at each frequency.

V. ORIENTATION MODE

The most intense peak in the HRS spectrum is the orientation mode at 0 cm^{-1} (also denoted as the hyper-Rayleigh peak) which is due to molecular orientation fluctuations. This has been studied recently and similar analysis is used for the vibration modes [39,40].

The T, L, and O orientation mode spectra were determined from HRS spectral scans with 1.24 and 4.2 cm^{-1} SSW (see Supplemental Material [30]). The T and L orientation mode spectra are narrow peaks with Lorentzian width $\Delta\nu_0 = 0.554\,\mathrm{cm}^{-1}$, while the O orientation mode spectrum is broader with a 2.2 cm^{-1} wide central peak. The measured Lorentzian width $\Delta\nu_0 = 0.554\,\mathrm{cm}^{-1}$ for the orientation mode gives relaxation time $\tau = (2\pi c\Delta\nu_0)^{-1} = 9.58$ ps. This is the same as the relaxation time determined by dielectric relaxation spectroscopy for D_2O at 29 °C [7], in agreement with the calculated temperature at the laser beam focus [30–33]. The 2.2 cm^{-1} octupolar spectral width is smaller than the $6 \times 0.554 = 3.3\,\mathrm{cm}^{-1}$ spectral width expected for orientation diffusion, but agrees with the $4 \times 0.554 = 2.2\,\mathrm{cm}^{-1}$ spectral

TABLE I. Relative intensities of O, T, and L modes of water for spectral bands with center frequency ν_c and bandwidth BW, with the uncertainty in the last digit given in parentheses. The 1 cm^{-1} BW results for D_2O are integrated intensity ratios for the narrow spectral components [30].

Sample	ν_c (cm^{-1})	BW (cm^{-1})	A_O/A_T	A_L/A_T
D_2O	0	1	0.17 (1)	0.017 (6)
	0	200	0.34 (1)	0.14 (1)
	400	600	3.98 (4)	8.73 (9)
	590	20	1.0 (2)	10.3 (7)
	1215	20	1.40 (6)	7.4 (2)
	2500	20	0.43 (6)	0.12 (2)
2 M KCl-D_2O	0	4	0.24 (4)	1.63 (3)
	0	200	0.73 (1)	1.50 (1)
	400	600	2.23 (2)	5.77 (6)
	590	20	1.6 (3)	12.3 (7)
	1215	20	1.9 (2)	5.0 (4)
	2500	20	1.3 (2)	0.3 (2)

width estimated using the extended jump model where hydrogen bond switching results in reorientation by large angular jumps [41,42]. For times short compared to the orientation relaxation time the configuration of the hydrogen bond network is disordered and random but fixed.

The dipolar orientation mode for pure D_2O is a nearly pure transverse mode, with the ratio $A_L/A_T = 0.017 \pm 0.006$ determined from the HRS spectra. A theoretical estimate for this ratio is obtained from the orientation correlation of the molecular dipoles in a molecular dynamics (MD) simulation using the TIP4P/2005 water model [39]. The theoretical spectral intensity ratio $S_L/S_T = 0.018$ in Table III of Ref. [39] is in good agreement with the experimental spectral intensity ratio $A_L/A_T = 0.017 \pm 0.006$. The interaction between the permanent molecular dipoles in the simulation produces a long-range pair correlation $B_L(r) = -2B_T(r) = (a/r)^3$ with $a = 0.166$ nm, where B_L and B_T are the orientation correlations longitudinal and transverse to the intermolecular vector. HRS polarized transverse to the scattering wave vector is calculated from the MD simulation results by summing the contributions of molecules with this long-range orientation correlation to distances at least as large as the wavelength of the scattering wave vector (284 nm in this experiment) [39].

Figure 2(b) shows the HRS spectra obtained for 2 M KCl solution. The orientational HRS spectra for pure D_2O and for 2 M KCl solution are the same except for a large intensity increase for the narrow peak at 0 cm^{-1} in the solution L spectrum. Table I shows that the dipolar orientation mode spectrum is mainly L polarized for the 2 M KCl solution, the result of long-range molecular orientation correlations induced by the radial electric field of the dissolved ions [43–46].

VI. VIBRATION MODES

The most prominent feature in Fig. 2(a) is the L mode peak at 568 cm^{-1}. This is assigned to combined rocking (tilt of C_{2v} axis with the molecular plane fixed) and wagging (tilt of C_{2v} axis and the molecular plane) modes of molecular libration, similar to rocking-wagging (rw) modes found in ice [18–20]. This is a dipolar mode since tilting the molecular axis modulates the molecular dipole vector and the vector component of β. A weaker T mode is also observed with peak at 540 cm^{-1}. The L-T mode splitting is 28 cm^{-1} with the L mode higher. The sign of the frequency difference is the same as for a dipole vibration mode, where the frequency for the mode with L polarized oscillating dipole is higher than for the T polarized mode. This indicates that both vector β and the oscillating dipole are L polarized for this HRS L mode. The opposite, L HRS with T polarized dipoles, was observed for $CDCl_3$ [29]. The dominant L mode intensity indicates long range correlation. Although a random isotropic vector field can be decomposed into L and T modes even if there is only short-range or even no correlation, correlation over distances as large as the wavelength of the scattering wave vector is required for the L and T mode intensities to become unequal.

The libration modes are heterogeneously broadened by the disorder of the hydrogen bond network. The curves fitted to the libration mode peak are a sum of Lorentzian functions to represent this broadening, and the long tails of these Lorentzian components add up to produce the sloping background extending from 800 to 2000 cm^{-1} that is seen in the VV HRS spectrum in Fig. 1. The intensity of the tail for a Lorentzian peak with width $\Delta\nu_j$ and fixed integrated intensity is proportional to $\Delta\nu_j$, so the sloping background carries information about the Lorentzian width. The sloping VV HRS background in Fig. 1 is produced mainly by the tails of the 72 cm^{-1} wide Lorentzian components fitting the T mode of the libration peak. The Lorentzian width that can fit both the libration peak and the sloping background is determined with about ± 20 cm^{-1} uncertainty. This 72 cm^{-1} lifetime broadened Lorentzian spectral width corresponds to a 74 fs relaxation time for the libration mode. This is consistent with the sub-100 fs decay of librational excitation in H_2O measured by a time resolved pump-probe experiment [47].

The next prominent feature in Fig. 2(a) is the O mode peak at 352 cm^{-1} which is assigned as the twisting libration (rotation around the C_{2v} axis). This motion does not modulate the dipole but does modulate the octupolar component of β.

Figure 2(a) also shows a weaker L mode with peak at 204 cm^{-1}, in the frequency range for hindered translation modes. However, a translation mode contribution to the L HRS spectrum requires modulation of vector β by the translation. This modulation can result from motion in the nonuniform electric field due to neighboring molecular dipoles, through the induced increment in the β tensor for a molecule given by

$$\Delta\beta_{ijk} = \gamma_{ijkl}E_l, \tag{10}$$

where γ is the second hyperpolarizability of the molecule and E is the electric field at the molecular site. The strong orientation correlation of nearest neighbors due to hydrogen bonding in water results in average field E in the same direction as the molecular dipole, which will result in a change in the average value of β for the molecule. Liquid phase β for water has the opposite sign compared to the gas phase value for β, and this has been investigated with successively more sophisticated models [48–51]. The results of combined molecular dynamics and high-level *ab initio* quantum chemical calculations in Refs. [48,49] indicate that Eq. (10) captures the main effect

of the liquid environment (but overestimates $\Delta\beta$ by a factor of 2–3 due to the strong inhomogeneity of E across each molecule).

Figure 2(b) shows that the translation mode HRS is much more intense in the 2 M KCl solution. This can result from modulation of $\Delta\beta$ as the molecules oscillate in the strong electric field gradient of nearby ions. The L peak at 171 cm^{-1} is accompanied by a weaker T peak at 155 cm^{-1}. The 16 cm^{-1} L-T splitting with the L mode higher indicates L polarization for both the oscillating dipole and $\Delta\beta$ of the L HRS mode. A mode at 46 cm^{-1} also appears in the L and T HRS spectra for the 2 M KCl solution that is absent in the pure D_2O HRS spectra. The Raman spectrum of water has peaks at 66 and 157 cm^{-1} assigned as translation modes [4], close to the T HRS frequencies. A study combining terahertz absorption measurements and molecular dynamics (MD) simulation for KCl solutions also finds modes at about 45 and 175 cm^{-1}, which are attributed to rattling of the ions within the water network [52].

The bending mode at 1215 cm^{-1} seen in Fig. 1 is mainly L polarized, with L peak at 1216 cm^{-1}, T peak at 1213 cm^{-1}, and LO-TO splitting 3 cm^{-1}. This indicates that both the oscillating dipole and $\Delta\beta$ for the L HRS mode are L polarized. The stretching mode at about 2500 cm^{-1} in Fig. 1 is strongly T polarized. This can be understood as the result of orientation correlation of the permanent molecular dipoles. The oscillating dipole for the symmetric stretching mode is oriented parallel to the permanent dipole of the molecule, so the oscillating dipoles for the stretching vibration will inherit the orientation correlation of the permanent molecular dipoles. This can account for the observed T polarization for the stretching mode, but not the L polarization of the bending mode. Long-range correlation for both bending and stretching vibrations is indicated by the unequal A_T and A_L intensities for these modes.

VII. DISCUSSION AND CONCLUSION

One result of the polarized HRS analysis is the dissection of the H-bond network band into distinct components: longitudinal polarized dipole modes at 568 and 171 cm^{-1}, their weaker transverse polarized companions at 540 and 155 cm^{-1}, and an octupolar mode at 352 cm^{-1}. The transverse HRS spectrum is consistent with the IR absorption spectrum for D_2O, which is sensitive only to transverse dipole modes, and has peaks at about 525 and 190 cm^{-1} [53,54]. The Raman scattering (RS) spectrum of D_2O has a broad band at 300−700 cm^{-1} and a narrow peak at 186 cm^{-1} [4,55]. The narrow peak for the hindered translation mode is intense in the RS spectrum but weak in the HRS spectrum. The broad band in the RS spectrum appears to be an unresolved sum of contributions from the T, L, and O libration modes of the HRS spectrum. Raman scattering is mediated by the second rank polarizability tensor α, which has even parity and can be expressed as the sum of irreducible spherical tensors of rank 0 and 2 (scalar and quadrupolar contributions), so RS and HRS report complementary information for each mode. Calculations of IR and Raman spectra based on *ab initio* molecular dynamics with 64 molecules are in fair agreement with the experimental IR and Raman spectra [14,56], so short-range interactions can account for the main features of the IR and Raman spectra, except that the calculation greatly overestimates the RS intensity for the libration band.

The second main result of the polarized HRS analysis is that all orientation and vibration modes of water are found to be collective with long-range correlation. The transverse and longitudinal dipole mode contributions dissected by HRS polarization analysis will have equal intensity unless there is correlation over distances comparable to the wavelength of the scattering wave vector. All the dipole modes are observed to be either dominantly transverse or longitudinal, which requires long-range correlation for the modes.

The dipole-dipole interaction between permanent molecular dipoles accounts for the long-range correlation of the transverse orientation mode in water [39]. Long-range correlation for the transverse stretching mode can be a consequence of the orientation mode correlation, since the transition dipole for the symmetric stretching vibration is parallel to the permanent dipole. However, the orientation correlation for the transverse polarized orientation mode cannot produce the long-range correlation for the translation, libration, and bending modes, which have opposite longitudinal polarization. A recent molecular dynamics simulation for water finds longitudinal optical phonons propagating at 2.7 km/s for the libration mode, and correlation effects for the libration mode out to the largest distances probed [9]. Phonon propagation is too slow to distribute correlation over distances of order 200 nm within the 74 fs lifetime for librational excitations. Direct coupling by electromagnetic fields would be fast enough to support the observed long-range correlation, but the mechanism is undetermined. Highly delocalized TO and LO modes similar to those in water have also been observed by HRS in the disordered network of silica glass [26,27]. Vibration modes with long-range correlation in disordered materials remains an unsolved problem, but such modes may be a common feature in liquids and glasses.

ACKNOWLEDGMENT

This work is supported by the National Science Foundation (USA) under Award No. CHE-1953941.

[1] F. Mallamace, C. Corsaro, and H. E. Stanley, Possible relation of water structural relaxation to water anomalies, Proc. Natl. Acad. Sci. USA **110**, 4899 (2013).

[2] A. K. Soper, F. Bruni, and M. A. Ricci, Site-site pair correlation functions of water from 25 to 400 °C: Revised analysis of new and old diffraction data, J. Chem. Phys. **106**, 247 (1997).

[3] T. Fukasawa, T. Sato, J. Watanabe, Y. Hama, W. Kunz, and R. Buchner, Relation between dielectric and low-frequency Raman spectra of hydrogen-bond liquids, Phys. Rev. Lett. **95**, 197802 (2005).

[4] D. M. Cary and G. M. Korenowski, Measurement of the Raman spectrum of liquid water, J. Chem. Phys. **108**, 2669 (1998).

[5] H. J. Baker and J. L. Skinner, Vibrational spectroscopy as a probe of structure and dynamics in liquid water, Chem. Rev. **110**, 1498 (2010).

[6] H. Elgabarty, T. Kampfrath, D. J. Bonthuis, V. Balos, N. K. Kaliannan, P. Loche, R. R. Netz, M. Wolf, T. K. Kuhne, and M. Sajadi, Energy transfer within the hydrogen bonding network of water following resonant terahertz excitation, Sci. Adv. **6**, eaay7074 (2020).

[7] B. Kutus, A. Shalit, P. Hamm, and J. Hunger, Dielectric response of light, heavy and heavy-oxygen water: Isotope effects on the hydrogen-bonding network's collective relaxation dynamics, Phys. Chem. Chem. Phys. **23**, 5467 (2021).

[8] P. A. Bopp, A. A. Kornyshev, and G. Sutmann, Frequency and wave-vector dependent dielectric function of water: Collective modes and relaxation spectra, J. Chem. Phys. **109**, 1939 (1998).

[9] D. C. Elton and M. Fernandez-Serra, The hydrogen-bond network of water supports propagating optical phonon-like modes, Nat. Commun. **7**, 10193 (2016).

[10] H. Torii, Dynamical behavior of molecular partial charges implied by the far-infrared spectral profile of liquid water, Chem. Phys. **512**, 165 (2018).

[11] S. Carlson, F. N. Brunig, P. Loche, D. J. Bonthuis, and R. R. Netz, Exploring the absorption spectrum of simulated water from MHz to infrared, J. Phys. Chem. A **124**, 5599 (2020).

[12] M. Sharma, R. Resta, and R. Car, Intermolecular dynamical charge fluctuations in water: A signature of the H-bond network, Phys. Rev. Lett. **95**, 187401 (2005).

[13] W. Chen, M. Sharma, R. Resta, G. Galli, and R. Car, Role of dipolar correlations in the infrared spectra of water and ice, Phys. Rev. B **77**, 245114 (2008).

[14] J. Xu, M. Chen, C. Zhang, and X. Wu, First-principles study of infrared spectrum in liquid water from a systematically improved description of H-bond network, Phys. Rev. B **99**, 205123 (2019).

[15] J. Xu, C. Zhang, L. Zhang, M. Chen, B. Santra, and X. Wu, Isotope effects in molecular structures and electronic properties of liquid water via deep potential molecular dynamics based on the SCAN functional, Phys. Rev. B **102**, 214113 (2020).

[16] K. Shiraga, Y. Fujii, A. Koreeda, K. Tanaka, T. Arikawa, and Y. Ogawa, Dynamic collectivity and nuclear quantum effects on the intermolecular stretching mode of liquid water, J. Phys. Chem. B **125**, 1632 (2021).

[17] D. Tisi, L. Zhang, R. Bertossa, H. Wang, R. Car, and S. Baroni, Heat transport in liquid water from first-principles and deep neural network simulations, Phys. Rev. B **104**, 224202 (2021).

[18] K. Abe, T. Miasa, Y. Ohtake, K. Nakano, M. Nakajima, H. Yamamoto, and T. Shigenari, Raman spectra of proton ordered XI phase ice crystal, J. Korean Phys. Soc. **46**, 300 (2005).

[19] P. Zhang, L. Tian, Z. P. Zhang, G. Shao, and J. C. Li, Investigation of the hydrogen bonding in ice Ih by first-principles density function methods, J. Chem. Phys. **137**, 044504 (2012).

[20] H. Itoh, K. Kawamura, T. Hondoh, and S. Mae, Polarized librational spectra of proton-ordered ice XI by molecular dynamics simulations, J. Chem. Phys. **109**, 4894 (1998).

[21] K. Iwano, T. Yokoo, M. Oguro, and S. Ikeda, Propagating librations in ice XI: Model analysis and coherent inelastic neutron scattering experiment, J. Phys. Soc. Jpn. **79**, 063601 (2010).

[22] P. Zhang, Z. Wang, Y.-B. Lu, and Z.-W. Ding, The normal modes of lattice vibrations of ice XI, Sci. Rep. **6**, 29273 (2016).

[23] V. N. Denisov, B. N. Mavrin, and V. B. Podobedov, Hyper-Raman scattering by vibrational excitations in crystals, glasses and liquids, Phys. Rep. **151**, 1 (1987).

[24] V. Korepanov, C.-C. Yu, and H.-o. Hamaguchi, Hyper-Raman investigation of intermolecular vibrations of water and ice, J. Raman Spectrosc. **49**, 1742 (2018).

[25] K. Inoue, Y. Litman, D. M. Wilkins, Y. Nagata, and M. Okuno, Is unified understanding of vibrational coupling of water possible? Hyper-Raman measurement and machine learning spectra, J. Phys. Chem. Lett. **14**, 3063 (2023).

[26] B. Hehlen and G. Simon, The vibrations of vitreous silica observed in hyper-Raman scattering, J. Raman Spectrosc. **43**, 1941 (2012).

[27] V. Rodriguez, New structural and vibrational opportunities combining hyper-Raman/hyper-Rayleigh and Raman scattering in isotropic materials, J. Raman Spectrosc. **43**, 627 (2012).

[28] D. P. Shelton, Long-range correlation of intra-molecular and inter-molecular vibration in liquid CCl_4, J. Chem. Phys. **154**, 034502 (2021).

[29] D. P. Shelton, Long range correlation of molecular orientation and vibration in liquid $CDCl_3$, AIP Adv. **12**, 105008 (2022).

[30] See Supplemental Material at http://link.aps.org/supplemental/10.1103/PhysRevB.108.174203 for experimental details on sample temperature, polarization and spectral analysis, and additional graphs of the data. It also contains Refs. [31–36].

[31] S. Kedenburg, M. Vieweg, T. Gissibl, and H. Giessen, Linear refractive index and absorption measurements of nonlinear optical liquids in the visible and near-infrared spectral region, Opt. Mater. Express **2**, 1588 (2012).

[32] J. P. Gordon, R. C. C. Leite, R. S. Moore, S. P. S. Porto, and J. R. Whinnery, Long-transient effects in lasers with inserted liquid samples, J. Appl. Phys. **36**, 3 (1965).

[33] A. Liñán and V. N. Kurdyumov, Laminar free convection induced by a line heat source, and heat transfer from wires at small Grashof numbers, J. Fluid Mech. **362**, 199 (1998).

[34] D. P. Shelton, Polarization and angle dependence for hyper-Rayleigh scattering from local and nonlocal modes of isotropic fluids, J. Opt. Soc. Am. B **17**, 2032 (2000); **34**, 1550(E) (2017).

[35] D. P. Shelton, Nonlocal hyper-Rayleigh scattering from liquid nitrobenzene, J. Chem. Phys. **132**, 154506 (2010).

[36] D. P. Shelton, Accurate hyper-Rayleigh scattering polarization measurements, Rev. Sci. Instrum. **82**, 113103 (2011).

[37] P. D. Maker, Spectral broadening of elastic second-harmonic light scattering in liquids, Phys. Rev. A **1**, 923 (1970).

[38] D. P. Shelton, Long-range correlation in dipolar liquids probed by hyper-Rayleigh scattering, J. Chem. Phys. **143**, 134503 (2015); **146**, 199901 (2017).

[39] D. P. Shelton, Structural correlation in water probed by hyper-Rayleigh scattering, J. Chem. Phys. **147**, 154501 (2017).

[40] D. P. Shelton, Long-range orientation correlation in water, J. Chem. Phys. **141**, 224506 (2014).

[41] D. Laage and J. T. Hynes, A molecular jump mechanism of water reorientation, Science **311**, 832 (2006).

[42] D. Laage and J. T. Hynes, On the molecular mechanism of water reorientation, J. Phys. Chem. B **112**, 14230 (2008).

[43] D. P. Shelton, Electric field of ions in solution probed by hyper-Rayleigh scattering, J. Chem. Phys. **130**, 114501 (2009).

[44] D. P. Shelton, Water-water correlations in electrolyte solutions probed by hyper-Rayleigh scattering, J. Chem. Phys. **147**, 214505 (2017).

[45] J. Duboisset and P.-F. Brevet, Salt-induced long-to-short range orientational transition in water, Phys. Rev. Lett. **120**, 263001 (2018).

[46] L. Belloni, D. Borgis, and M. Levesque, Screened Coulombic orientation correlations in dilute aqueous electrolytes, J. Phys. Chem. Lett. **9**, 1985 (2018).

[47] S. Ashihara, N. Huse, A. Espagne, E. T. J. Nibbering, and T. Elsaesser, Ultrafast structural dynamics of water induced by dissipation of vibrational energy, J. Phys. Chem. A **111**, 743 (2007).

[48] G. L. Breton, O. Bonhomme, E. Benichou, and C. Loison, First hyperpolarizability of water in bulk liquid phase: Long-range electrostatic effects included via the second hyperpolarizability, Phys. Chem. Chem. Phys. **24**, 19463 (2022).

[49] C. Liang, G. Tocci, D. M. Wilkins, A. Grisafi, S. Roke, and M. Ceriotti, Solvent fluctuations and nuclear quantum effects modulate the molecular hyperpolarizability of water, Phys. Rev. B **96**, 041407(R) (2017).

[50] Y. Foucaud, J.-F. Dufreche, B. Siboulet, M. Duvail, A. Jonchere, O. Diat, and R. Vuilleumeier, Why local and non-local terms are essential for second harmonic generation simulation?, Phys. Chem. Chem. Phys. **24**, 12961 (2022).

[51] K. V. Mikkelsen, Y. Luo, H. Agren, and P. Jorgensen, Sign change of hyperpolarizability of solvated water, J. Chem. Phys. **102**, 9362 (1995).

[52] D. A. Schmidt, O. Birer, S. Funkner, B. P. Born, R. Gnanasekaran, G. W. Schwaab, D. M. Leitner, and M. Havenith, Rattling in the cage: Ions as probes of sub-picosecond water network dynamics, J. Am. Chem. Soc. **131**, 18512 (2009).

[53] J.-J. Max and C. Chapados, Isotope effects in liquid water by infrared spectroscopy. III. H_2O and D_2O spectra from 6000 to 0 cm^{-1}, J. Chem. Phys. **131**, 184505 (2009).

[54] Y. Marechal, The molecular structure of liquid water delivered by absorption spectroscopy in the whole IR region completed with thermodynamic data, J. Mol. Struct. **1004**, 146 (2011).

[55] M. H. Brooker, G. Hancock, B. C. Rice, and J. Shapter, Raman frequency and intensity studies of liquid H_2O, $H_2{}^{18}O$ and D_2O, J. Raman Spectrosc. **20**, 683 (1989).

[56] G. M. Sommers, M. F. C. Andrade, L. Zhang, H. Wang, and R. Car, Raman spectrum and polarizability of liquid water from deep neural networks, Phys. Chem. Chem. Phys. **22**, 10592 (2020).